

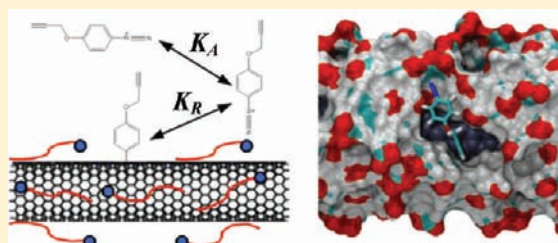
# Molecular Perspective on Diazonium Adsorption for Controllable Functionalization of Single-Walled Carbon Nanotubes in Aqueous Surfactant Solutions

Shangchao Lin,<sup>†,§</sup> Andrew J. Hilmer,<sup>†</sup> Jonathan D. Mendenhall,<sup>†</sup> Michael S. Strano,<sup>†</sup> and Daniel Blankschtein<sup>\*,†</sup>

<sup>†</sup>Department of Chemical Engineering and <sup>§</sup>Department of Mechanical Engineering, Massachusetts Institute of Technology, Cambridge, Massachusetts 02139, United States

**S** Supporting Information

**ABSTRACT:** Functionalization of single-walled carbon nanotubes (SWCNTs) using diazonium salts allows modification of their optical and electronic properties for a variety of applications, ranging from drug-delivery vehicles to molecular sensors. However, control of the functionalization process remains a challenge, requiring molecular-level understanding of the adsorption of diazonium ions onto heterogeneous, charge-mobile SWCNT surfaces, which are typically decorated with surfactants. In this paper, we combine molecular dynamics (MD) simulations, experiments, and equilibrium reaction modeling to understand and model the extent of diazonium functionalization of SWCNTs coated with various surfactants (sodium cholate, sodium dodecyl sulfate, and cetyl trimethylammonium bromide). We show that the free energy of diazonium adsorption, determined using simulations, can be used to rank surfactants in terms of the extent of functionalization attained following their adsorption on the nanotube surface. The difference in binding affinities between linear and rigid surfactants is attributed to the synergistic binding of the diazonium ion to the local “hot/cold spots” formed by the charged surfactant heads. A combined simulation–modeling framework is developed to provide guidance for controlling the various sensitive experimental conditions needed to achieve the desired extent of SWCNT functionalization.



## 1. INTRODUCTION

Selective adsorption of solutes onto a charged solid surface in an aqueous medium is a generic process utilized across industries and technologies,<sup>1–3</sup> which is often difficult to predict and control. Conventional continuum-based theories (e.g., the Langmuir isotherm and the Poisson–Boltzmann equation<sup>4</sup>) neglect the atomic-scale properties of the solute and the surface and, therefore, cannot be used to elucidate and molecularly predict many important adsorption phenomena. Among the properties neglected, surface heterogeneity<sup>5</sup> and surface-charge mobility<sup>6</sup> both contribute to the discrete and dynamic nature of the adsorption process. For example, amorphous silica (SiO<sub>2</sub>) substrates present surfaces with high roughness and nonuniformly distributed charges.<sup>5</sup> In a more complex scenario, ionic surfactant-covered solid surfaces exhibit both surface roughness and charge-mobility, because the surfactant molecules can diffuse freely on the surface while adsorbed.<sup>7–10</sup> Many solution-phase chemical processes involve the use of surfactants to disperse and decorate solid nanoparticles, including single-walled carbon nanotubes (SWCNTs).<sup>11</sup>

The surface roughness of surfactant-covered SWCNTs results from the molecular “islands” formed by agglomerated surfactant assemblies on the surface.<sup>8,12,13</sup> Such a surface is also charge-mobile (in the case of ionic surfactants), since the

charged surfactant head groups can move freely on the surface.<sup>8,12</sup> Studying these features at the molecular level can provide insight into useful methods to control the functionalization of SWCNTs.<sup>14,15</sup> There has been a significant recent interest in developing methods to functionalize the nanotube sidewall, such that the nanotube optical and electronic properties can be modified for a variety of applications,<sup>16</sup> ranging from drug-delivery vehicles<sup>17</sup> to molecular sensors.<sup>18,19</sup> Among various functionalization methods used, reaction with diazonium salts (see Figure 1d) represents a promising route for the covalent modification of the SWCNT.<sup>11</sup> Although this functionalization method involves covalent reaction of the negatively charged diazonium ion with the neutral sp<sup>2</sup> carbon atoms on the nanotube sidewall, it has been proposed that the step which is selective toward functionalization is the noncovalent adsorption/binding of the diazonium ion on the nanotube surface (see Figure 1e for a schematic of the two-step functionalization process).<sup>20</sup> Recently, we have demonstrated that, by decorating the SWCNT with different surfactants (sodium cholate (SC), sodium dodecyl sulfate (SDS), and cetyl trimethyl ammonium bromide (CTAB) (see a, b, and c,

Received: February 18, 2012

Published: April 24, 2012

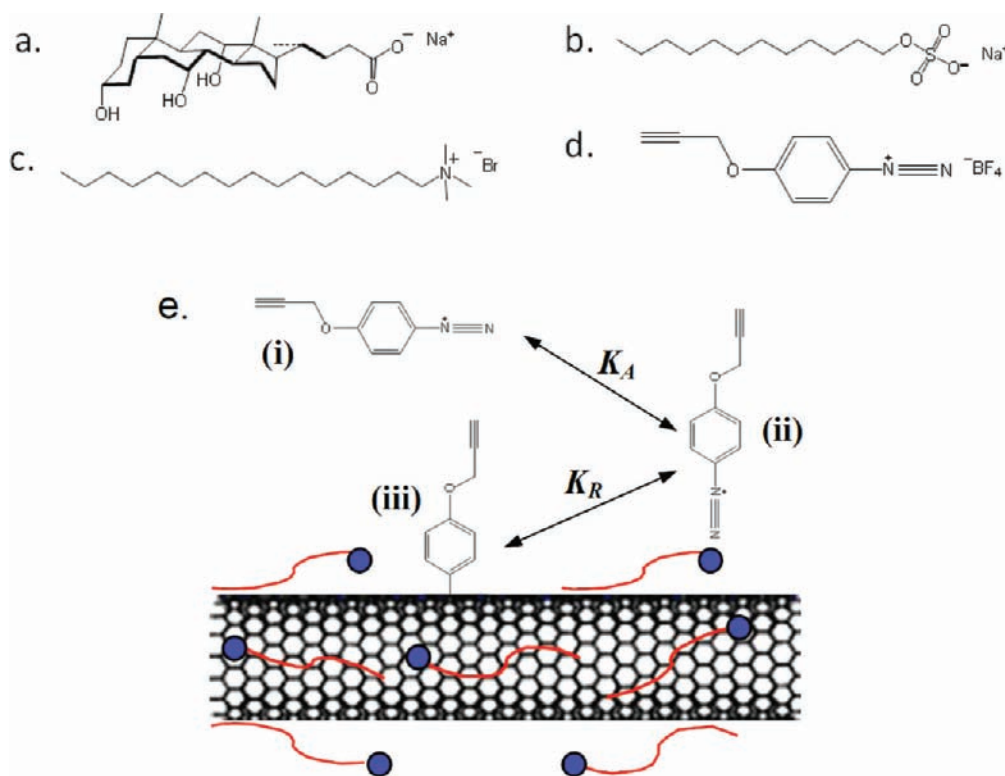


**Figure 1.** Chemical structures of the surfactants and the diazonium salt considered in this study: (a) sodium cholate (SC), (b) sodium dodecyl sulfate (SDS), (c) cetyl trimethylammonium bromide (CTAB), and (d) tetrafluoroborate ( $\text{BF}_4^-$ ) aryl diazonium. The bile salt SC has rigid steroidal backbones, which results in hydrophobic and hydrophilic “faces”. Therefore, SC can also be referred to as a “facial” surfactant. The rigidity of the SC molecules leads them to form a monolayer structure on the nanotube surface.<sup>8</sup> The flexible linear surfactants, SDS and CTAB, possess less rigid, hydrophobic chains, which tend to coat the nanotube in a more disordered manner at high surface coverages.<sup>12</sup> (e) Schematic of the equilibrium model proposed here, showing the three possible states of the diazonium ion during the functionalization process: (i) free in the surfactant aqueous solution, (ii) adsorbed on the SWCNT–surfactant complex (with an adsorption constant  $K_A$ ), and (iii) covalently bound to the SWCNT surface (with a reaction constant  $K_R$ ). Adsorbed surfactant molecules are shown as blue beads (the hydrophilic surfactant heads) connected with red lines (the hydrophobic surfactant tails).

respectively, of Figure 1), one can control the extent of functionalization.<sup>15</sup>

With the above in mind, in this contribution, we combine molecular dynamics (MD) simulations, experiments, and equilibrium reaction modeling to understand and model the extent of diazonium functionalization of SWCNTs coated with SC, SDS, and CTAB. A combined simulation-modeling framework is presented that can be used to guide the control of various sensitive experimental conditions needed to achieve the desired extent of SWCNT functionalization.

## 2. METHODS

**2.1. Simulation Methods.** Molecular dynamics (MD) simulations of diazonium ion adsorption onto the SWCNT–surfactant complex in aqueous solution were carried out using the GROMACS 4.0 software package.<sup>21</sup> The (6,6) SWCNT was first covered with surfactants (SC, SDS, or CTAB) which were fully dissociated into surfactant ions and counterions ( $\text{Na}^+$  in the case of SC and SDS, and  $\text{Br}^-$  in the case of CTAB). Low and high surfactant surface coverages, having linear packing densities of 2.44 and 5.85 surfactants per nm of the SWCNT, respectively, as utilized in recent simulation studies,<sup>12,13</sup> were chosen to investigate coverage effects on binding affinities. For comparison, the experimentally estimated linear packing densities of SDS,<sup>22</sup> SC,<sup>23</sup> and CTAB<sup>15</sup> are  $4.5 \pm 1.0$ ,  $3.6 \pm 1.0$ , and  $10 \pm 1.0$  molecules/nm, respectively. The equilibrated

SWCNT–surfactant configurations corresponding to these surface coverages were generated using the same simulation method described in our recent simulation work on the SWCNT–SC assembly, where each simulation ran for more than 100 ns.<sup>8</sup> The simulation parameters used in this study and the force-field parameters for water, the SWCNT, and SC were also drawn from ref 8. Note that a thermostat of 45 °C was utilized for all the simulations in order to match the experimental conditions. The alkane tails of SDS and CTAB were modeled using the OPLS-AA force-field,<sup>24</sup> with updated dihedral parameters.<sup>25</sup> The sulfate head of SDS and its connection to the dodecyl tail were modeled following Lopes et al.,<sup>26</sup> while the trimethylammonium head of CTAB and its connection to the cetyl tail were modeled following Lopes and Pádua.<sup>27</sup> Note that the surfactant head-related force-field parameters developed by Pádua and co-workers were specifically developed in a manner that is consistent with the use of the OPLS-AA force field for each surfactant tail.<sup>26,27</sup>

The tetrafluoroborate anion ( $\text{BF}_4^-$ ) of the aryl diazonium salt was modeled using the force-field parameters in ref 26. The atomic charges of the positively charged diazonium ion were not previously available in the literature, and were generated using the quantum mechanics (QM) software package, Gaussian 03,<sup>28</sup> together with the CHELPG electrostatic potential-fitting algorithm<sup>29</sup> at the MP2/cc-pVTZ(-f)//HF/6-31G\* level of theory. This level of theory was selected for the purpose of maintaining consistency with the models of Lopes et

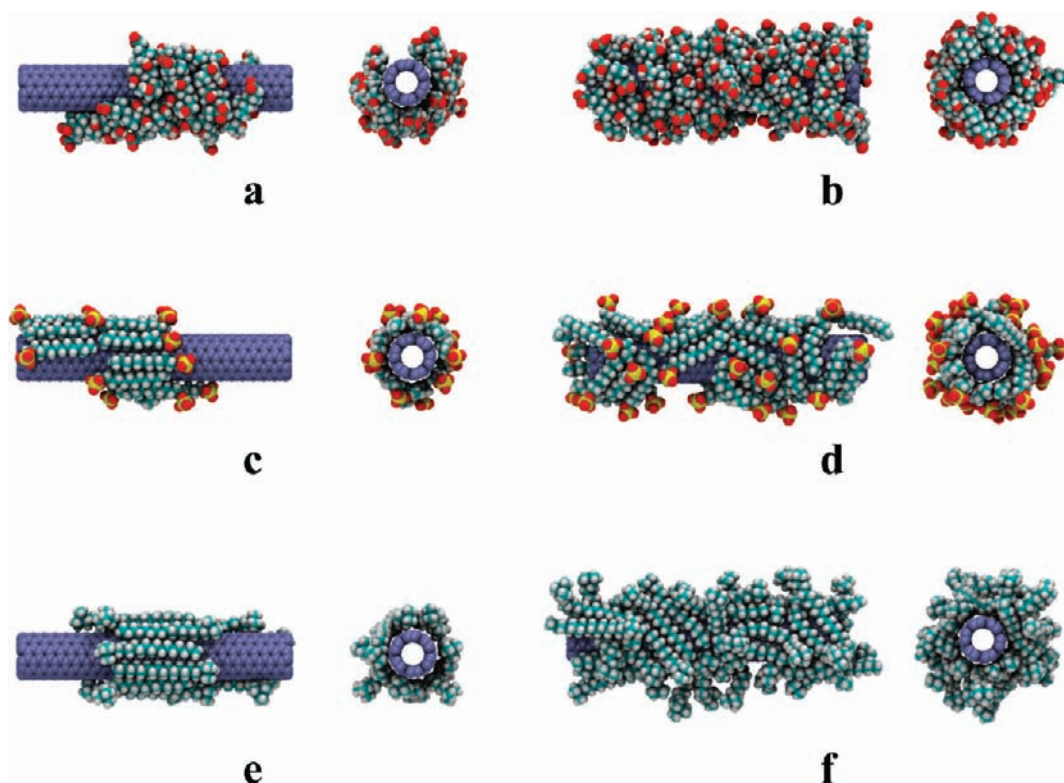


**Figure 2.** Postequilibrium simulation snapshots of SWCNTs covered with surfactants, showing the surface structures of the various surfactants considered here. (a) and (b) for the SC case, (c) and (d) for the SDS case, and (e) and (f) for the CTAB case. Within each row, the side view is on the left, and the front view is on the right. (a), (c), and (e) correspond to low surfactant surface coverages, while (b), (d), and (f) correspond to high surfactant surface coverages. Water molecules and counterions are not shown for clarity. Color code: red – oxygen, light blue – carbon, white – hydrogen, dark blue – nitrogen, and purple – carbon in the SWCNT.

al.<sup>26,27,30</sup> The cc-pVTZ(-f) basis set was adapted from the cc-pVTZ basis set of Dunning,<sup>31</sup> as provided at the Basis Set Exchange,<sup>32,33</sup> by removing the  $d$  polarization function from hydrogen and the  $f$  polarization functions from heavier atoms.<sup>30</sup> All other force-field parameters for the diazonium ion were drawn from the OPLS-AA force field. The computed partial atomic charges of the diazonium ion are summarized in Table S1 in Supporting Information.

The interactions between the diazonium ion and the SWCNT–surfactant complex were quantified using the simulated potential of mean force (PMF). The case where no surfactants are present, corresponding to the bare SWCNT in water, was also investigated for comparison. To mimic the infinite dilution of the diazonium salt in the actual experiments, only one diazonium ion was introduced in the simulation cell. The diazonium ion was constrained at various radial positions,  $r$ , relative to the cylindrical axis ( $z$ -axis) of the SWCNT, and allowed to move freely on each concentric cylindrical surface around the nanotube (see Figure 3). We also monitored the coordinates of the diazonium ion as a function of simulation time (see Figure S1 in Supporting Information), which confirmed that the diazonium ion can move freely along, as well as around, the SWCNT for given  $r$  values. The simulation at each  $r$  value was equilibrated for 40 ns before recording the mean force (averaged over another 20 ns),  $\langle f(r) \rangle$ , that is required to constrain the center of mass (COM) of the diazonium ion at each  $r$  value. Note that the 40 ns equilibration time is necessary to allow the surfactant molecules to diffuse along the SWCNT surface to form local “hot spots” around the diazonium ion when approaching the nanotube (see section 3.2

for details). The PMF, as a function of  $r$ , was obtained by numerically integrating  $\langle f(r) \rangle$  along  $r$ . Specifically,<sup>15</sup>

$$\text{PMF}(r) = \int_d^r \langle f(r) \rangle dr + k_B T \ln(r/d) \quad (1)$$

where  $d$  is the largest separation distance along  $r$ ,  $k_B$  is the Boltzmann constant, and  $T = 318$  K is the temperature in degrees Kelvin. Note that  $k_B T \ln(r/d)$  accounts for the entropy loss of the diazonium ion resulting from the decrease in the area of the concentric surface from  $2\pi dL$  to  $2\pi rL$ , where  $L$  is the length of the simulated SWCNT. Different initial diazonium ion configurations (different molecular orientations as well as different positions on the SWCNT cylindrical surface) were tested to ensure that the PMF results were independent of the initial configuration.

**2.2. Experimental Methods.** Diazonium–SWCNT functionalizations in aqueous SDS and SC solutions were carried out by preheating 2 and 3 mL, respectively, of 15 mg/L SWCNT dispersion samples at pH = 5 to 45 °C, allowing them to stabilize at that temperature, and initiating the functionalization by single additions of diazonium salt to the well-stirred vessel. The solutions were then allowed to react for 24 h, at which point there was negligible residual diazonium ions in solution. Due to the repulsive interactions between the positively charged SWCNT–CTAB complex and the positively charged diazonium ion, the diazonium–SWCNT reactions in the aqueous CTAB solution took significant longer time to reach completion. The above functionalization was carried out at 27 °C and pH = 5 in 2 mL of 15 mg/L SWCNT dispersion sample, and initiated by a single addition of diazonium salt.

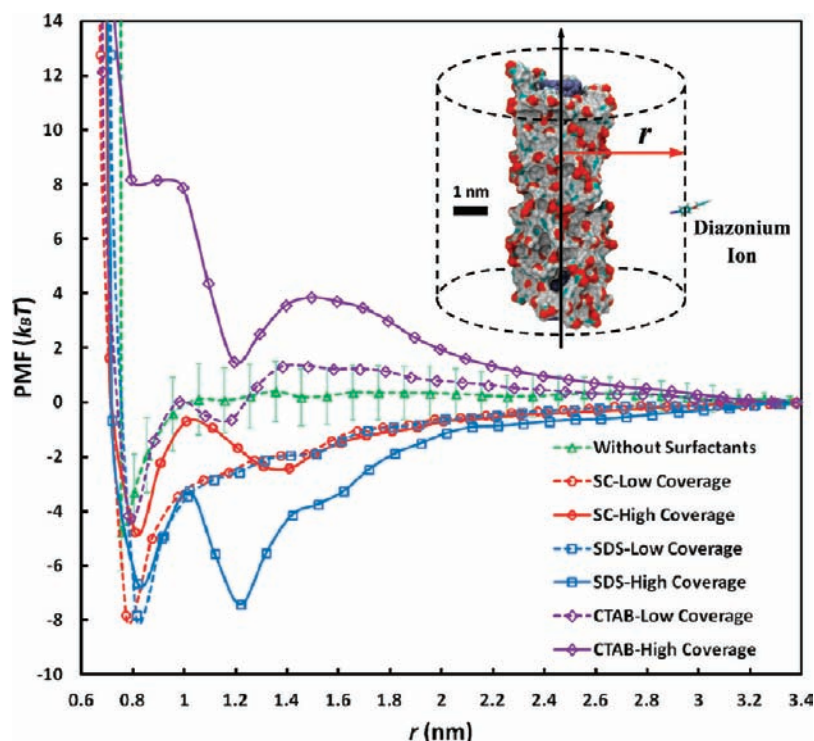


**Figure 3.** Simulated PMF profiles between the diazonium ion and the SWCNT–surfactant complexes corresponding to SC, SDS, and CTAB for both low and high surface coverages. The no surfactant case (that is, the bare SWCNT in water) is also shown for comparison. The error bars in green, corresponding to the simulated no surfactant case, represent the typical errors in our PMF calculations for the surfactant cases simulated here ( $<2k_B T$ ). The inset shows a schematic drawing of the cylindrical axis ( $z$ -axis) of the SWCNT (the black arrow), the constraint distance,  $r$ , between this axis and the diazonium ion (the red arrow), and the cylindrical surface on which the diazonium ion can move freely (the black dashed lines). The simulation snapshot of the high surface coverage SWCNT–SC complex is used here. Water molecules and counterions are not shown for clarity. The color code is the same as the one used in Figure 2.

Samples were allowed to react for 2.5 weeks, at which point there was little residual diazonium ions in the solution. Photoluminescence (785 nm excitation) data were acquired using a home-built near-infrared fluorescence microscope which has been described elsewhere.<sup>34</sup> Deconvolution of the photoluminescence (PL) spectra allowed for more accurate analysis of the fractional quenching behavior of the (7,5) nanotube considered in this study (see Supporting Information).

### 3. RESULTS AND DISCUSSION

**3.1. Free-Energy Calculations of Diazonium Ion Adsorption.** The surface self-assembly structures formed by several surfactants (e.g., SDS, SC, and SDBS (sodium dodecyl benzene sulfonate)) on SWCNTs have been studied previously using all-atomistic MD simulations.<sup>8,12,13,35</sup> The simulated surface structures of the SWCNT–surfactant complexes considered here (SC, SDS, and CTAB which is simulated for the first time) are shown in Figure 2. Our simulated surface self-assembly structures are consistent with those reported earlier for both the flexible surfactant (SDS)<sup>12</sup> and the rigid surfactant (SC)<sup>8</sup> at low and high surface coverages on a (6,6) SWCNT.

The simulated potential of mean force (PMF) profiles between the single diazonium ion and the SWCNT–surfactant complexes are shown in Figure 3. For  $r > 1.8$  nm, where the diazonium ion has very weak interactions with the SWCNT–surfactant complex through short-range van der Waals (vdW) forces (reflected in the Lennard-Jones model),<sup>8</sup> the long-range electrostatic interactions between the diazonium cation and the

charged SWCNT–surfactant complexes dominate. Note that the interaction force between the diazonium ion and the SWCNT–surfactant complex is related to the slope of the PMF along  $r$ , because it is equal to the derivative of the PMF along  $r$  (see eq 1). By convention, the attractive force is related to a positive slope and the repulsive force is related to a negative slope. As expected, the electrostatic forces exerted on the diazonium cation by the negatively charged SWCNT–surfactant (SC and SDS) complexes are attractive, with the PMF profile exhibiting a positive slope (see the red solid and dashed lines for SC, as well as the blue solid and dashed lines for SDS in Figure 3). On the other hand, these forces are repulsive in the case of the positively charged SWCNT–surfactant (CTAB) complex, with the PMF profile exhibiting a negative slope (see the purple solid and dashed lines in Figure 3). For comparison, the force exerted on the diazonium ion by the uncharged, bare SWCNT in water is almost zero, with a horizontal PMF profile (see the green dashed line in Figure 3). The different surface charge densities corresponding to the low and high surface coverages affect the strength of the long-range electrostatic interactions; however, these differences are negligible for large  $r$  values where the electrostatic interactions are relatively weak.

As the diazonium ion approaches the SWCNT–surfactant complex before establishing direct contacts with the complex ( $1.2 \text{ nm} < r < 1.8 \text{ nm}$ ), the strong vdW attraction between the diazonium ion and the SWCNT–surfactant complex comes into play, and favors adsorption of the diazonium ion. Note that the adsorption of the diazonium ion first occurs onto the coated surfactant layers rather than directly onto the nanotube

**Table 1. Summary of Parameter Values for  $A = P\theta_{\text{TR}}$ ,  $\theta_{\text{TA}}$ , and  $K_{\text{R}}$  in eq 9 by Fitting to the Experimental Values of  $C_0$  and  $f_{(m,n)}^i$  (see Figure 6a) with constants  $l$  and  $K_{\text{A}}$  using the simulated  $\Delta G_{\text{A}}$  values in eq 4**

surfactant type	$l$ (nm)	$\Delta G_{\text{A}}$ ( $k_{\text{B}}T$ )	$K_{\text{A}}$	$A = P\theta_{\text{TR}}$	$\theta_{\text{TA}}$	$K_{\text{R}}$
SC	$2.26 \times 10^{16}$	$-4.8 \pm 2.0$	$1.22 \times 10^2$	0.105	$7.49 \times 10^{-20}$	$9.35 \times 10^{23}$
SDS	$1.505 \times 10^{16}$	$-7.4 \pm 2.0$	$1.64 \times 10^3$	1.000	$1.05 \times 10^{-19}$	$9.22 \times 10^{23}$
CTAB	$1.505 \times 10^{16}$	$1.5 \pm 1.0$	$2.23 \times 10^{-1}$	0.292	$7.65 \times 10^{-21}$	$1.24 \times 10^{27}$

surface. This results in a local free-energy minimum at  $r = 1.2$  nm (for SDS and CTAB, with a vdW radius of  $\sim 0.25$  nm for the cross-sectional area of the linear alkyl tail) or 1.4 nm (for SC, because of its larger molecular size as a rigid surfactant, with a thickness of  $\sim 0.45$  nm for the bean-like molecule<sup>8</sup>). Note that the adsorption discussed here is clearly seen only at high surfactant surface coverages, because at low surfactant surface coverages the attractive and the repulsive forces are both weak. Indeed, the PMF profiles for SC and SDS corresponding to the low surfactant surface coverages are very similar (see the red and the blue dashed lines in Figure 3), reflecting a lack of molecular discrimination between different surfactants of the same charge when the diazonium ions adsorb on low surface coverage SWCNT–surfactant complexes. Interestingly, however, one observes a much larger increase in the attraction between the positively charged diazonium ion and the high surface coverage, negatively charged SWCNT–SDS complex than in the case of the high surface coverage, negatively charged SWCNT–SC complex (see the red and the blue solid lines in Figure 3). This stronger attraction is surprising because the electrostatic contribution to the PMF profile is expected to be similar for the same surfactant surface coverage (or surface charge density), as expected from the conventional Poisson–Boltzmann equation<sup>4</sup> for SWCNT–surfactant complexes with similar radii (discussed further in section 3.2). The resulting local free-energy well depth is  $-7.4 \pm 2.0 k_{\text{B}}T$  at  $r = 1.2$  nm in the case of SDS, and  $-2.4 \pm 2.0 k_{\text{B}}T$  at  $r = 1.4$  nm in the case of SC. This clearly shows that the binding affinity of the diazonium ion on the surfactant layer of the SWCNT–SDS complex is much stronger (by  $-5.0 k_{\text{B}}T$ ) than that on the SWCNT–SC complex.

For  $r < 1.2$  nm (for SDS and CTAB) and  $r < 1.4$  nm (for SC), the diazonium ion begins to push away the adsorbed surfactant molecules in order to contact the SWCNT surface directly, which results in the free-energy barrier for all the surfactant cases considered within the range  $1.0 \text{ nm} < r < 1.2$  nm (see Figure 3). Direct contact of the diazonium ion on the SWCNT surface results in the local free-energy minima observed at  $r = 0.8$  nm (again, for all the surfactant cases considered). For  $r < 0.8$  nm, the repulsive force between the diazonium ion and the SWCNT increases sharply, as clearly seen in Figure 3.

A quantitative measure of the free energy associated with the diazonium ion adsorption (prior to any covalent reaction),  $\Delta G_{\text{A}}$ , corresponds to the lowest PMF value at which the diazonium ion adsorbs stably onto the surfactant layer (for SDS and CTAB, both at  $r = 1.2$  nm) or directly onto the SWCNT (for SC, at  $r = 0.8$  nm). This difference in the stably adsorbed positions may be due to the competing effects between electrostatic, vdW, and steric interactions for the different surfactant cases. Experimentally, surfactants are typically added into the SWCNT solution at saturation levels. Consequently, we utilized the simulated PMF profiles corresponding to the high surface coverage SWCNT–surfactant complexes to determine the value of  $\Delta G_{\text{A}}$  for SDS, CTAB, and SC. Although

it has been proposed that the covalent reaction of the diazonium ions with the  $sp^2$  carbons on the nanotube sidewall occurs directly on the SWCNT surface, contact of the diazonium ions with the surfactant layers may still affect the reaction with the SWCNT. In fact, the actual reaction pathway corresponding to the SWCNT–surfactant complex functionalization by diazonium salts is still unknown, and therefore, the definition of the free energy of diazonium adsorption presented here should be viewed as an approximate quantitative measure, with additional reaction-pathway studies required in the future. The simulated  $\Delta G_{\text{A}}$  values are listed in Table 1 for the SC, SDS, and CTAB cases. The negative  $\Delta G_{\text{A}}$  values for SC ( $-4.8 \pm 2.0 k_{\text{B}}T$ ) and SDS ( $-7.4 \pm 2.0 k_{\text{B}}T$ ) indicate preferential adsorption of diazonium ions onto SWCNTs. On the other hand, the positive  $\Delta G_{\text{A}}$  value for CTAB ( $1.5 \pm 1.0 k_{\text{B}}T$ ) indicates preferential desorption of diazonium ions from the SWCNTs. Overall, the binding affinity ( $K_{\text{A}}$ , see eq 3 in section 3.3) of the diazonium ions on various SWCNT–surfactant complexes ranks as follows: SDS > SC > CTAB, while the experimental extent of diazonium functionalization (see section 3.3 for the definition) is ranked as follows: SDS > CTAB > SC (see Figure 5a). This discrepancy (the switch between CTAB and SC) indicates that covalent reactions between diazonium ions and SWCNTs, in addition to noncovalent adsorptions, may also be affected by the surfactants used, and will be discussed further in section 3.3.

### 3.2. Understanding the Synergetic Binding Affinity.

To better understand the role of surfactants in determining the ranking of the  $\Delta G_{\text{A}}$  values using the simulated PMF profile, we calculated the interaction potential energies between the diazonium ion and the SC, SDS, and CTAB molecules adsorbed onto the SWCNT surface at high surfactant surface coverages as a function of  $r$ . The calculated potential energy profiles in Figure 4a capture the main feature of the PMF profile in Figure 3, showing that the SDS curve (blue line) lies below the SC curve (red line), which reflects the stronger interaction (having a more negative potential energy value) between the diazonium ion and the SDS molecules than between the diazonium ion and the SC molecules. In addition, the CTAB curve (green line) lies above both the SC and the SDS curves, which reflects the weakest interaction (having more positive potential energy values) between the diazonium ion and the CTAB molecules. This ranking of the magnitudes of the potential energies (SDS > SC > CTAB) is fully consistent with that of the predicted binding affinities based on the free energies of adsorption. This indicates that the potential energy contribution to the free energy of adsorption is dominant, compared to other contributions such as the solvent effect (e.g., the confinement of water molecules between the diazonium ion and the SWCNT–surfactant complex), or the entropic effect (e.g., the orientational entropy of water molecules around the diazonium ion and the surfactant molecules, and the orientational entropy of the diazonium ion itself). Note that the various minima and maxima observed

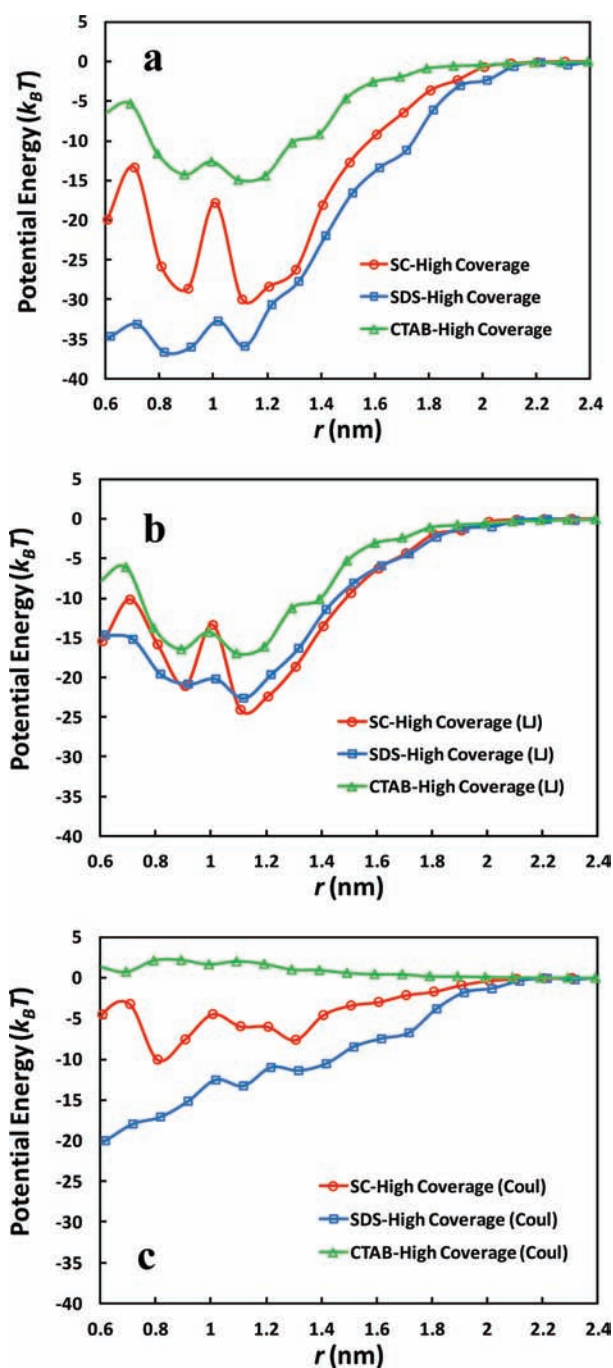


**Figure 4.** (a) Interaction potential energy between the diazonium ion and SC, SDS, and CTAB molecules adsorbed on the SWCNT surface at high surfactant surface coverages, as a function of  $r$ . (b) The Lennard-Jones (LJ) contribution to the potential energy in (a), which reflects both the vdW and the steric interactions between the diazonium ion and the surfactant molecules. (c) The Coulombic (Coul) contribution to the potential energy in (a), which reflects the electrostatic interactions between the diazonium ion and the surfactant molecules.

in Figure 4a are consistent with those in Figure 3, with similar features being observed in b and c of Figure 4.

The potential energy was further decomposed into Lennard-Jones (LJ) and Coulombic (Coul) contributions, as shown in b and c of Figure 4, respectively. Note that the vdW and steric interactions are reflected in the LJ contribution, while the electrostatic interactions are reflected in the Coul contribution.

As shown in Figure 4b, the LJ contributions to the potential energies for SC, SDS, and CTAB are relatively close (within  $5 k_B T$  from each other), exhibiting various overlaps for the three curves. On the other hand, in Figure 4c, the Coul contributions are quite different from each other, with positive values for the positively charged CTAB molecules (which repel the diazonium ion) and negative values for the negatively charged SDS and SC molecules (which attract the diazonium ion). The clear ranking of the binding affinities due to the Coul contribution (SDS > SC > CTAB) is fully consistent with that of the predicted binding affinities based on the free energies of adsorption. This finding confirms that the primary contribution to the binding affinities of the diazonium ions with the SWCNT–surfactant complexes is electrostatic.

We would like to better understand the unexpected, strong binding affinity between the diazonium ion and the SWCNT–SDS complex relative to that corresponding to the SWCNT–SC complex, with particular emphasis on the role of the electrostatic interaction which, as shown above, are the dominant ones. As discussed earlier, SWCNT surfaces covered with surfactants are heterogeneous, with mobile charges carried by the surfactant heads. It is therefore important to monitor how these mobile charges distribute as a diazonium ion approaches the SWCNT–surfactant complex. A useful way developed here to visualize the charge distribution involves using simulated density maps of the charged surfactant head groups (carboxylate for SC, sulfate for SDS, and trimethylammonium for CTAB) projected onto an unrolled, two-dimensional, flat SWCNT surface. The simulated density maps are shown in Figure 5, where each map has been centered at the position of the charged diazo group ( $-N^+ \equiv N$ ) of the diazonium ion, as projected on the SWCNT surface.

For  $r = 3.3$  nm, the density maps are very similar for the three surfactants considered, demonstrating a homogeneous distribution of the surfactant head groups. This is expected, since the diazonium ion is not close enough to the SWCNT surface to affect the surface organization of the surfactant molecules via electrostatic interactions. For  $r = 1.7$  nm, the diazonium ion begins to interact with the surfactant molecules directly through the formation of ionic bonds (attractive for SC and SDS, and repulsive for CTAB),<sup>15</sup> similar to the formation of a salt bridge in the case of counterion binding.<sup>4</sup> The ionic bonding is even stronger when the diazonium ion can approach the SWCNT–surfactant complex closer to make direct contact at  $r = 1.1$  nm, as reflected by the increase in the extents of both the “hot spots” (high surfactant head density) and “cold spots” (low surfactant head density). This reflects the increase in the synergistic electrostatic interaction (attractive for “hot spots” and repulsive for “cold spots”) between the diazo group and the surfactant heads. Note, however, that ionic bonding is only apparent for the linear surfactants (SDS and CTAB, see the  $r = 1.1$  nm column in Figure 5), and not for the rigid surfactant (SC, see the  $r = 1.1$  nm column in Figure 5). Indeed, as shown in the  $r = 1.1$  nm column in Figure 5, the cationic diazo group attracts anionic SDS sulfate groups (brighter ring), while it repels cationic CTAB trimethylammonium groups (appears as a dark hole in the plot, since the origin of the density map is always occupied by the diazo group itself at small  $r$  values).

In the case of SC (see the middle row in Figure 5), for  $r = 1.7$  or  $1.1$  nm, we did not observe any “hot spots” for the carboxylate head groups around the diazo group, although one can observe a small extent of ordering of the carboxylate groups at  $r = 1.1$  nm. Synergistic electrostatic attractions between the

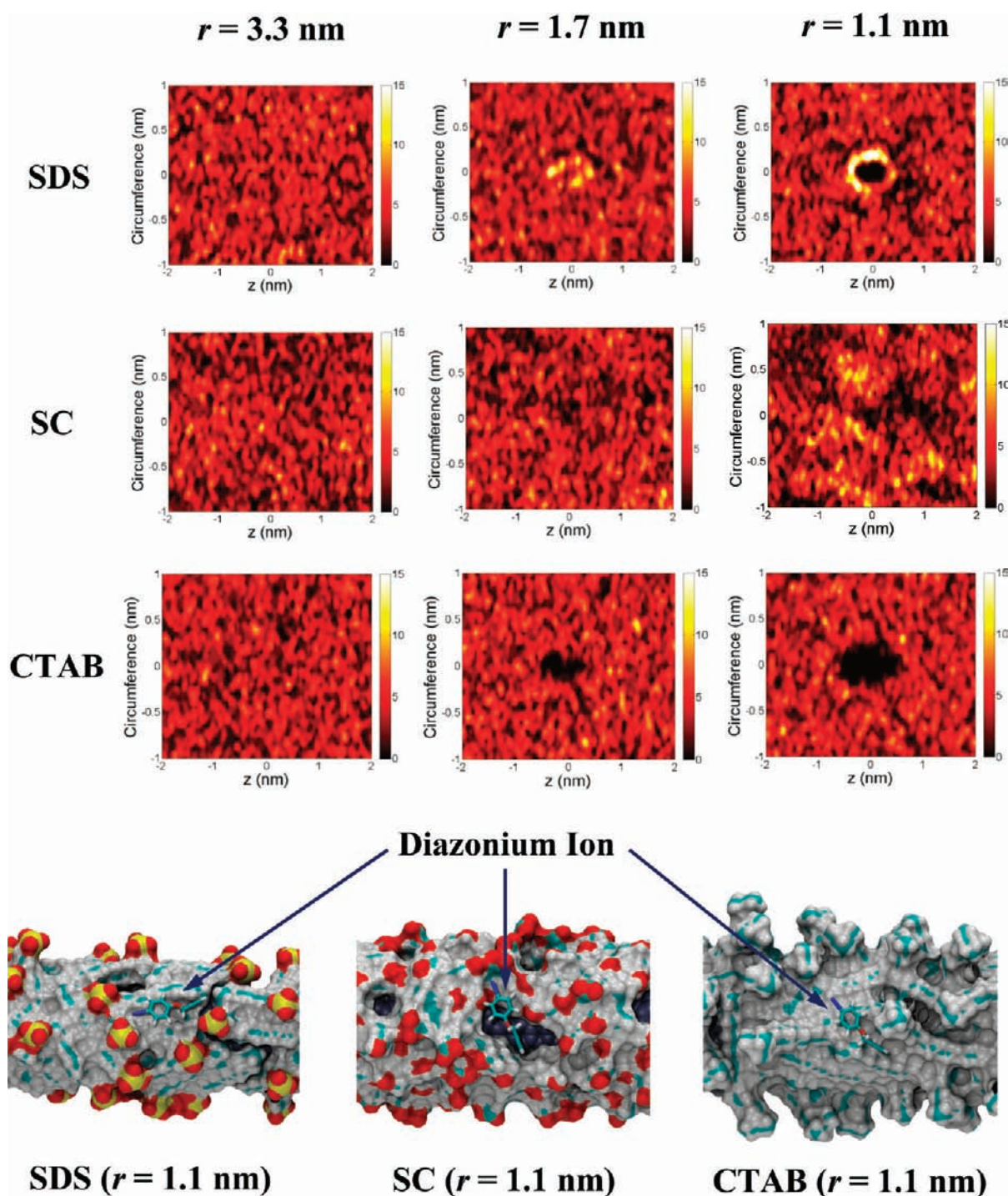


**Figure 5.** Projected density maps of charged surfactant head groups on the unrolled SWCNT surface (tube length  $\times$  tube circumference) for: SDS (top row), SC (middle row), and CTAB (bottom row). Within each plot, the diazonium ion approaches the SWCNT–surfactant complex gradually from the left to the right, where the left subplot,  $r = 3.3$  nm; middle subplot,  $r = 1.7$  nm; and right subplot,  $r = 1.1$  nm. The  $y$ -axis measures the circumference of the SWCNT, and the  $z$ -axis measures the length of the SWCNT. Density maps are shown as contour plots with arbitrary units. Color bar code: lighter color corresponds to high surfactant head densities, and darker color corresponds to low surfactant head densities. The origin of each plot at  $y = z = 0$  denotes the projected position of the charged diazo group ( $-N^+ \equiv N$ ) of the diazonium ion. Each density map was averaged over the last 20 ns of each simulation. Representative simulation snapshots showing the binding of the diazonium ion (the blue arrows) to the charged surfactant layer on the SWCNT surface are shown at the bottom of the density maps corresponding to  $r = 1.1$  nm. The color code is the same as the one used in Figure 2. Note that the diazonium ion and the various SWCNT–surfactant complexes are drawn in the “Licorice” and the “Surf” representation in VMD,<sup>54</sup> respectively, to facilitate distinction between the two.

cationic diazo group and the anionic SDS and SC head groups lead to the rearrangement of these surfactant molecules on the SWCNT surface, leading to their localization around the

diazonium ion, and giving rise to the local “hot spots”. This surface rearrangement can maximize the contacts of the anionic SDS and SC molecules with the cationic diazo group, thereby

lowering the free energy of the system. On the other hand, antagonistic electrostatic repulsions occur between the cationic diazo group and the cationic CTAB head groups, giving rise to the local “cold spots”. Our finding that the linear, flexible SDS molecules can rearrange on the SWCNT surface more readily than the bulkier, rigid SC molecules and thereby generate a greater extent of “hot spots” formation is consistent with our recently reported numbers of ionic bonds formed between the diazo groups and the head groups of SDS ( $\sim 2.4$  at  $r = 1.1$  nm) and SC ( $\sim 1.5$  at  $r = 1.1$  nm),<sup>15</sup> which can serve as a quantitative measure of the local “hot spots”. The three representative simulation snapshots at the bottom of Figure 5 show the close binding of the diazonium ion to the charged surfactant layer (SDS, SC, and CTAB) on the SWCNT surface at  $r = 1.1$  nm. The diazonium ion lies in parallel to the SWCNT surface when closely bound to the surfactant layer. Its orientation relative to the SWCNT axis is not fixed, and it depends on the detailed self-assembly structure of the surfactant layer.

### 3.3. Model for the Extent of SWCNT Functionalization.

We have recently modeled kinetic properties, such as reaction rates associated with the diazonium–SWCNT functionalization process, by combining a diffusion-limited model and the Poisson–Boltzmann equation.<sup>15</sup> Here, we focus on modeling the equilibrium (steady-state) extent of diazonium–SWCNT functionalization using our simulated free energies of adsorption and experimental data. It is noteworthy that the simulated free energy of adsorption may be used to replace the Poisson–Boltzmann equation when combined with the diffusion-limited model in order to predict kinetic properties, such as the aggregation rate, as we have shown recently.<sup>9,36</sup> Specifically, we propose the following two-step adsorption–reaction model for the diazonium–SWCNT functionalization process (see Figure 1e), a description that is more general than that presented in ref 20. Specifically,



where  $C$  denotes the bulk concentration of the diazonium salt (in units of diazonium/water molar ratio),  $\theta_{EA}$  denotes the number of empty adsorption sites available to the diazonium ions on the nanotube surface (in units of diazonium/water molar ratio per nm, which is a linear packing density on the SWCNT surface),  $\theta_A$  denotes the number of sites occupied by the adsorbed diazonium ions,  $\theta_{ER}$  denotes the number of empty reaction sites available to the diazonium ions, and  $\theta_R$  denotes the number of sites occupied by the reacted diazonium ions (where the units of  $\theta_A$ ,  $\theta_{ER}$ , and  $\theta_R$  are the same as that of  $\theta_{EA}$ ),  $K_A$  is the adsorption constant, and  $K_R$  is the reaction constant. Unlike the previous model,<sup>15</sup> we assume that the adsorbed diazonium ions can react with the carbon atoms on the SWCNT sidewall reversibly in order to investigate the equilibrium reaction properties (e.g.,  $\theta_{ER}$ ,  $\theta_R$ , and  $K_R$ ).

Knowing  $\Delta G_A$ , the simulated free energy of adsorption (i.e., the free-energy difference between the adsorbed and the desorbed states), which can be obtained from the PMF calculations, the adsorption constant,  $K_A$ , can be determined using Arrhenius' law, in order to relate  $C$ ,  $\theta_{EA}$ , and  $\theta_A$ . Specifically,

$$K_A = \frac{\theta_A}{C\theta_{EA}} = e^{-\Delta G_A/k_B T} \quad (4)$$

The total number of available adsorption sites on the nanotube,  $\theta_{TA}$ , is given by  $\theta_{TA} = \theta_{EA} + \theta_A$ . Since the reaction is carried out at infinite dilution of the diazonium salt, it follows that  $\theta_{TA} \gg \theta_A$ , which leads to  $\theta_{EA} \approx \theta_{TA}$ . Using this result in eq 4, it follows that:

$$\theta_A = K_A \theta_{TA} C \quad (5)$$

Note that eq 5 is the celebrated Henry's adsorption isotherm, where  $K_A$  is Henry's constant. Note also that the bulk concentration of the diazonium salt,  $C$ , decreases as the number of adsorbed diazonium ions,  $\theta_A$ , increases. This observation can be expressed as follows:  $C = C_0 - l \theta_A$ , where  $C_0$  is the initial concentration of the diazonium salt added to the SWCNT solution, and  $l$  is the total length of the SWCNTs in the solution. Note that the effect of adsorption on the value of  $C$  cannot be neglected, because  $l$  is typically quite large. Using the expression for  $C$  in terms of  $C_0$  and  $l$  in eq 5, and rearranging results in:

$$\theta_A = \frac{K_A \theta_{TA} C_0}{1 + K_A \theta_{TA} l} \quad (6)$$

The total number of available reaction sites on the nanotube,  $\theta_{TR}$ , is given by  $\theta_{TR} = \theta_{ER} + \theta_R$ . Unlike the adsorption step,  $\theta_R$  is not negligible relative to  $\theta_{TR}$ . Therefore, the reaction step associated with the reaction constant,  $K_R$ , may be modeled using a Langmuir isotherm. It is important to recognize that the incorporation of a ceiling for reaction,  $\theta_{TR}$ , is essential in order to capture the quenching saturation phenomenon as  $C_0$  increases.<sup>15</sup> Indeed, this saturation phenomenon cannot be simply explained by the diazonium adsorption process, as described using the linear relationship in eq 6. Specifically,

$$K_R = \frac{\theta_R}{\theta_A \theta_{ER}} = \frac{\theta_R}{\theta_A (\theta_{TR} - \theta_R)} \Rightarrow \theta_R = \frac{K_R \theta_A}{1 + K_R \theta_A} \theta_{TR} \quad (7)$$

Experimentally, the equilibrium extent of functionalization,  $f_{(m,n)}^i$ , as a function of both the carbon nanotube type (i.e., chirality),  $(m,n)$ , and the surfactant type,  $i$ , was estimated from the fractional quenching data in the PL spectra (the change in the PL intensity after functionalization, normalized by the original intensity).<sup>15</sup> Here, as proof-of-concept, we have only investigated one carbon nanotube species (7,5), with diameter  $d = 0.81$  nm, and  $i =$  CTAB, SDS, and SC. Since we are only considering a single nanotube species, differences in electronic structure, across nanotube species, are not relevant to the physical adsorption of the diazonium ions. As a result,  $K_A$ ,  $K_R$ ,  $\theta_{TA}$ , and  $\theta_{TR}$  are only functions of the nanotube diameter,  $d$ , and the surfactant type,  $i$ . Note that the simulated (6,6) SWCNT has almost the same tube diameter as the (7,5) SWCNT, and therefore, can be utilized to approximate the (7,5) SWCNT disregarding the difference in chirality. This is suggested in a recent simulation study showing that surfactants adsorbed on a graphite surface are highly disordered without any orientation preference for chirality angles.<sup>10</sup> Assuming that each diazonium ion contributes the same extent of PL quenching to the total extent of PL quenching, we can relate the extent of functionalization considered here,  $f_{(7,5)}^i$ , to the reacted diazonium surface coverage,  $\theta_R$ , through a simple

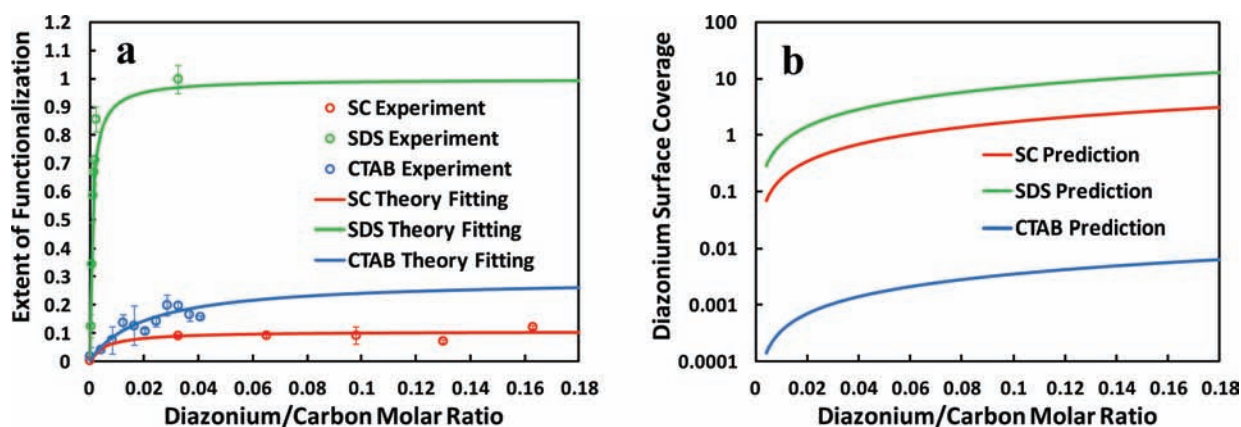


**Figure 6.** (a) Experimental data (circles) and theoretical fitting results (solid lines) for the extents of functionalization ( $f_{(7,5)}^{SC}$ ,  $f_{(7,5)}^{SDS}$ , and  $f_{(7,5)}^{CTAB}$ ) as a function of the diazonium/carbon molar ratio. The solid lines were predicted using eq 9, and the corresponding fitting parameters are listed in Table 1. (b) Predicted diazonium ion surface coverage (adsorption isotherm),  $\theta_A$  (in units of number of diazonium ions per nm of a SWCNT), as a function of the diazonium/carbon molar ratio, using eq 6 and the fitting parameters listed in Table 1.

proportionality relationship, with a proportionality constant  $P$  (in units of nm per diazonium/water molar ratio). Specifically,

$$f_{(7,5)}^i = P\theta_R \quad (8)$$

By substituting eqs 6 and 7 into eq 8, we can obtain a master equation that relates  $f_{(7,5)}^i$  to various parameters. Specifically:

$$\begin{aligned} f_{(7,5)}^i &= \frac{P\theta_{TR}\theta_{TA}K_RK_A C_0}{1 + \theta_{TA}K_RK_A C_0 + \theta_{TA}K_A l} \\ &= \frac{AK_RK_A C_0}{1/\theta_{TA} + K_RK_A C_0 + K_A l} \end{aligned} \quad (9)$$

where  $A = P\theta_{TR}$ , which is equal to the saturated (or maximum) extent of functionalization,  $\max(f_{(7,5)}^i)$ , as  $C_0$  approaches infinity. Note that  $K_A$  can be predicted using the simulated  $\Delta G_A$  values for each surfactant type, and  $C_0$  is tuned experimentally. On the other hand, estimates of  $A$ ,  $\theta_{TA}$ , and  $K_R$  are not available directly from either simulations or experiments. Fortunately, we can obtain these three unknown parameters by fitting eq 9 to the available experimental data for the diazonium-functionalized (7,5) SWCNTs in SC, SDS, and CTAB solutions ( $f_{(7,5)}^{SC}$ ,  $f_{(7,5)}^{SDS}$ , and  $f_{(7,5)}^{CTAB}$ ), respectively. The resulting fitting curves for various  $C_0$  values are shown in Figure 6a. Note that, in Figure 6a, the  $C_0$  value was converted into diazonium/carbon (one carbon atom in the SWCNT) molar ratio, according to the carbon/water molar ratio of  $2.25 \times 10^{-5}$  (for the 15 mg/L SWCNT solution used here). Specifically, the  $l$  values were estimated from the total mass of the SWCNTs (see section 2.2), and the number of carbon atoms in the SWCNT per unit length ( $\sim 100$  atoms/nm for the (7,5) SWCNT as a rough approximation).

**3.4. Modeling Results and Discussions.** The deduced fitting parameters,  $A$ ,  $\theta_{TA}$ , and  $K_R$  are listed in Table 1, demonstrating the ability of eq 9 to model the concentration-dependent extent of functionalization shown in Figure 6a. The nonlinear minimization algorithm for the least-squares fitting was carried out utilizing the interior-reflective Newton method subroutine in the MATLAB numerical library. The fitted  $A$  values (i.e.,  $\max(f_{(7,5)}^i)$ ) are ranked as follows: SDS > CTAB > SC, consistent with the experimental extents of functionalization shown in Figure 6a. The higher  $A$  value for CTAB than for SC indicates that, although the anionic surfactant SC yields a larger diazonium binding affinity than the cationic surfactant

CTAB, diazonium ions adsorbed and subsequently reacted on the SWCNT–CTAB complex can quench the PL intensity more effectively. This effectiveness may be due to the fact that the diazonium reaction can occur randomly along the nanotube for the linear surfactant CTAB, while it occurs very close to a preoccupied reaction site for the rigid surfactant SC. As shown in Figure 5, CTAB (or any other linear surfactant) molecules are more likely to restructure for the diazonium ion to adsorb randomly on the nanotube surface. On the other hand, this is less likely for SC molecules, which leads to multiple diazonium reactions occurring within the same PL-quenched region along the nanotube (i.e., less effectiveness per reacted diazonium ion). This leads to the discrepancy in the rankings of the simulated  $K_A$  values and the experimental extents of functionalization for the different surfactant cases considered, as stressed in section 3.1.

The fitted  $\theta_{TA}$  values are ranked as follows: SDS > SC > CTAB, consistent with the ranked  $K_A$  values in section 3.1. The fitted  $K_R$  values for the two anionic surfactants (SC and SDS) are very similar ( $\sim 10^{24}$ ), while the  $K_R$  value for CTAB is much larger ( $\sim 10^{27}$ ). This  $K_R$  difference suggests that cationic surfactants may modify the electronic structure of the SWCNT upon adsorption, which in turn, would enhance the reactivity of the SWCNT with the diazonium ions. The fitted  $K_R$  value corresponds to the free energy of diazonium–SWCNT reaction (determined using Arrhenius' law similar to eq 4),  $\Delta G_R = -55 k_B T$  ( $-1.40$  eV) for SC and SDS, and  $\Delta G_R = -62 k_B T$  ( $-1.59$  eV) for CTAB, which are consistent with the QM simulated binding energy for the desorption process of phenyl from bare (5,5) SWCNT ( $-1.42$  eV).<sup>37</sup> In addition, note that  $K_R$  is much larger than  $K_A$ , which indicates that the reaction of the diazonium ion with the SWCNT sidewall is highly favorable, a finding which is consistent with the previously proposed irreversible reaction step.<sup>20</sup>

Although estimates of  $A = P\theta_{TR}$  are not available experimentally, there is experimental evidence that each individual reacted diazonium ion on the nanotube sidewall (referred to as a quenching site) can quench the PL intensity (excitons generated upon photon excitation) of every 100–300 nm of nanotube.<sup>38–40</sup> This length along the nanotube,  $\Lambda$ , is referred to as the effective mean quenching range of a single reacted diazonium ion.<sup>39</sup> Fundamentally,  $\Lambda$  can also be referred to as the exciton diffusion range for the functionalized

SWCNT, a range for which an exciton can travel during its lifetime.<sup>38</sup> Experimental evidence based on time-dependent PL intensities (exciton kinetics) have shown that the value of  $\Lambda$  depends on both the SWCNT chirality<sup>40</sup> and the surfactant (e.g., SC, SDBS, SDC (sodium deoxycholate), and STC (sodium taurocholate)) utilized to disperse the SWCNT.<sup>39</sup> From the experimentally estimated value of  $\Lambda = 178 \pm 20$  nm per reacted diazonium ion for (7,5) SWCNTs dispersed in an aqueous SC solution,<sup>39</sup> we can estimate the corresponding proportionality constant  $P$  in eq 8. Specifically,

$$P = \Lambda N_{\text{water}} \quad (10)$$

where  $N_{\text{water}}$  is the number of water molecules in the SWCNT solution, which is about  $10^{23}$  for the 3 mL aqueous SC solution (see section 2.2). In addition, based on the relation that  $A = P\theta_{\text{TR}}$ , we can estimate the corresponding value of  $\theta_{\text{TR}}$ . Specifically,

$$\theta_{\text{TR}} = \frac{A}{P} = \frac{A}{\Lambda N_{\text{water}}} \quad (11)$$

Using the values of  $\Lambda$  and  $N_{\text{water}}$  given above in eqs 10 and 11, we find that:  $P = 1.78 \times 10^{25}$  nm per diazonium/water molar ratio, and  $\theta_{\text{TR}} = 5.90 \times 10^{-27}$  diazonium/water molar ratio per nm (or  $\sim 6$  reacted diazonium ions per  $10^4$  nm of the SWCNT). The predicted  $\theta_{\text{TR}}$  value is 7 orders of magnitude smaller than the  $\theta_{\text{TA}}$  value ( $7.49 \times 10^{-20}$  diazonium/water molar ratio per nm), which reflects the fact that very few physically adsorbed diazonium ions will eventually react with the nanotube sidewall to form covalent bonds. If experimental values of  $\Lambda$  were available for SDS and CTAB, we would also be able to accurately predict the corresponding  $P$  and  $\theta_{\text{TR}}$  values. As an order of magnitude estimation, the values of  $P$  and  $\theta_{\text{TR}}$  should be  $\sim 10^{25}$  nm per diazonium/water molar ratio, and 1 to 10 reacted diazonium ions per  $10^3$  nm of the SWCNT, respectively, regardless of the surfactant type and the SWCNT species.

Using the fitted values of  $A$ ,  $\theta_{\text{TA}}$ , and  $K_{\text{R}}$  in eq 6, we can independently predict the surface coverage (adsorption isotherm) of the diazonium ions on the various SWCNT–surfactant complexes (see Figure 6b). The predicted surface coverage profiles are consistent with the ranked  $K_{\text{A}}$  and  $\theta_{\text{TA}}$  values for SDS, SC, and CTAB. As can be seen, the predicted surface coverages span 5 orders of magnitude (from 0.0001 to 10 diazonium ions per nm of the SWCNT). This clearly shows the ability of the various surfactants considered to modify the adsorption of diazonium ions. In addition, it implies that the functionalization process is extremely sensitive to the use of surfactants. In general, the theoretical framework developed here can also be utilized to model other surfactant types,  $i$ , SWCNT chiralities,  $(m,n)$ , and experimental conditions (e.g., SWCNT and diazonium salt concentrations, ionic strengths, pHs, and temperatures). This would require establishing a large database that contains  $K_{\text{A}}$  values as a function of  $i$  and  $(m,n)$  from simulations, as well as  $A$ ,  $\theta_{\text{TA}}$ , and  $K_{\text{R}}$  values as a function of  $i$  and  $(m,n)$  obtained by fitting the model to the available experimental data.

## 4. CONCLUSIONS

In this contribution, we combined molecular dynamics (MD) simulations, experiments, and equilibrium reaction modeling to both understand and model the extent of diazonium functionalization of SWCNTs coated with various surfactants.

The free energy associated with diazonium adsorption determined from the PMF calculations using simulations can be used to rank surfactants in terms of the extent of functionalization upon their decoration on the nanotube surface. The distinct binding affinities between linear and rigid surfactants were further investigated in detail, and attributed to the synergetic binding of the diazonium ion to the local “hot spots” formed by the accumulated, charged surfactant heads. Finally, a general theoretical framework was developed, which explicitly takes into account the reversibility of the diazonium reaction and the extensive diazonium adsorption on SWCNTs. This combined simulation-modeling framework can provide molecular-level information on quantities involved in the adsorption and reaction of diazonium ions with SWCNTs, which are very difficult to obtain or quantify through experiments. In addition, it can help understand the complex functionalization process, and guide the various sensitive experimental procedures to achieve the desired extent of SWCNT functionalization.

It is important to note that the theoretical framework presented here is not restricted to diazonium functionalization of SWCNTs, but can be extended, in general, to model solid surfaces (e.g., graphene,<sup>41,42</sup> graphene oxide,<sup>43,44</sup> silicon,<sup>45</sup> silica,<sup>5,46</sup> metal,<sup>45–47</sup> metal oxide,<sup>48</sup> etc.) functionalized by any agent with complex molecular structures. The heterogeneous nature of many solid surfaces (e.g., those with surfactant/polymer coatings,<sup>9,49</sup> having amorphous structures,<sup>5,44</sup> or having random defects<sup>50,51</sup>) can be modeled very well by molecular simulations. The proposed modeling framework that combines simulations with theoretical models can be utilized in a creative way to understand, at the molecular level, phenomena which involve physical adsorption, chemical adsorption, or both.<sup>52,53</sup>

## ■ ASSOCIATED CONTENT

### 📄 Supporting Information

Table S1, Figure S1, method for deconvoluting SWCNT fluorescence spectra, and complete ref 28. This material is available free of charge via the Internet at <http://pubs.acs.org>.

## ■ AUTHOR INFORMATION

### Corresponding Author

dblank@mit.edu

### Notes

The authors declare no competing financial interest.

## ■ ACKNOWLEDGMENTS

S.L., J.D.M., and D.B. are grateful for the financial support from the DuPont–MIT Alliance and the National Science Foundation (Contract No. CBET-1133813). Computational resources were partially supported by the Atlantic Computational Excellence Network (ACEnet) in Canada. A.J.H. acknowledges funding from the Department of Energy SCGF program (Contract No. DE-AC05-06OR23100). We thank Professor Pak K. Yuet, Chih-Jen Shih, Jaisree Iyer, and Vishnu Sresht for helpful discussions.

## ■ REFERENCES

- (1) Regnier, F. E.; Gooding, K. M. *Anal. Biochem.* **1980**, *103*, 1.
- (2) Movileanu, L.; Niedzwiecki, D. J.; Grazul, J. *J. Am. Chem. Soc.* **2010**, *132*, 10816.

- (3) Tegenfeldt, J. O.; Prinz, C.; Cao, H.; Huang, R. L.; Austin, R. H.; Chou, S. Y.; Cox, E. C.; Sturm, J. C. *Anal. Bioanal. Chem.* **2004**, *378*, 1678.
- (4) Hiemenz, P. C.; Rajagopalan, R. *Principles of Colloid and Surface Chemistry*, 3rd ed.; Marcel Dekker: New York, 1997.
- (5) Carr, R.; Comer, J.; Ginsberg, M. D.; Aksimentiev, A. *J. Phys. Chem. Lett.* **2011**, *2*, 1804.
- (6) Israelachvili, J. N. *Intermolecular and Surface Forces*, 3rd ed.; Academic Press: Burlington, MA, 2010.
- (7) Tummala, N. R.; Striolo, A. *J. Phys. Chem. B* **2008**, *112*, 1987.
- (8) Lin, S.; Blankschtein, D. *J. Phys. Chem. B* **2010**, *114*, 15616.
- (9) Lin, S.; Shih, C.-J.; Strano, M. S.; Blankschtein, D. *J. Am. Chem. Soc.* **2011**, *133*, 12810.
- (10) Sammalkorpi, M.; Panagiotopoulos, A. Z.; Haataja, M. *J. Phys. Chem. B* **2008**, *112*, 2915.
- (11) Strano, M. S.; Dyke, C. A.; Usrey, M. L.; Barone, P. W.; Allen, M. J.; Shan, H. W.; Kittrell, C.; Hauge, R. H.; Tour, J. M.; Smalley, R. E. *Science* **2003**, *301*, 1519.
- (12) Tummala, N. R.; Striolo, A. *ACS Nano* **2009**, *3*, 595.
- (13) Xu, Z. J.; Yang, X. N.; Yang, Z. *Nano Lett.* **2010**, *10*, 985.
- (14) Blanch, A. J.; Lenehan, C. E.; Quinton, J. S. *J. Phys. Chem. C* **2012**, *116*, 1709.
- (15) Hilmer, A. J.; McNicholas, T. P.; Lin, S.; Zhang, J.; Wang, Q. H.; Mendenhall, J. D.; Song, C.; Heller, D. A.; Barone, P. W.; Blankschtein, D.; Strano, M. S. *Langmuir* **2012**, *28*, 1309.
- (16) Schnorr, J. M.; Swager, T. M. *Chem. Mater.* **2010**, *23*, 646.
- (17) Kostarelos, K.; Bianco, A.; Prato, M. *Nat. Nanotechnol.* **2009**, *4*, 627.
- (18) Lin, Y.; Lu, F.; Tu, Y.; Ren, Z. *Nano Lett.* **2003**, *4*, 191.
- (19) Cai, H.; Cao, X.; Jiang, Y.; He, P.; Fang, Y. *Anal. Bioanal. Chem.* **2003**, *375*, 287.
- (20) Usrey, M. L.; Lippmann, E. S.; Strano, M. S. *J. Am. Chem. Soc.* **2005**, *127*, 16129.
- (21) Hess, B.; Kutzner, C.; van der Spoel, D.; Lindahl, E. *J. Chem. Theory Comput.* **2008**, *4*, 435.
- (22) Grossiord, N.; van der Schoot, P.; Meuldijk, J.; Koning, C. E. *Langmuir* **2007**, *23*, 3646.
- (23) Arnold, M. S.; Suntivich, J.; Stupp, S. I.; Hersam, M. C. *ACS Nano* **2008**, *2*, 2291.
- (24) Jorgensen, W. L.; Maxwell, D. S.; Tirado-Rives, J. *J. Am. Chem. Soc.* **1996**, *118*, 11225.
- (25) Jorgensen, W. L.; Price, M. L. P.; Ostrovsky, D. *J. Comput. Chem.* **2001**, *22*, 1340.
- (26) Lopes, J. N. C.; Padua, A. A. H.; Shimizu, K. *J. Phys. Chem. B* **2008**, *112*, 5039.
- (27) Lopes, J. N. C.; Padua, A. A. H. *J. Phys. Chem. B* **2004**, *108*, 16893.
- (28) Frisch, M. J.; et al. *Gaussian 03*, Revision C.02, Gaussian, Inc.: Wallingford CT, 2004.
- (29) Breneman, C. M.; Wiberg, K. B. *J. Comput. Chem.* **1990**, *11*, 361.
- (30) Lopes, J. N. C.; Deschamps, J.; Padua, A. A. H. *J. Phys. Chem. B* **2004**, *108*, 2038.
- (31) Dunning, T. H. *J. Chem. Phys.* **1989**, *90*, 1007.
- (32) Schuchardt, K. L.; Didier, B. T.; Elsethagen, T.; Sun, L. S.; Gurumoorathi, V.; Chase, J.; Li, J.; Windus, T. L. *J. Chem. Inf. Model.* **2007**, *47*, 1045.
- (33) Feller, D. *J. Comput. Chem.* **1996**, *17*, 1571.
- (34) Barone, P. W.; Yoon, H.; Ortiz-Garcia, R.; Zhang, J. Q.; Ahn, J. H.; Kim, J. H.; Strano, M. S. *ACS Nano* **2009**, *3*, 3869.
- (35) Suttipong, M.; Tummala, N. R.; Kitiyanan, B.; Striolo, A. *J. Phys. Chem. C* **2011**, *115*, 17286.
- (36) Shih, C.-J.; Lin, S.; Strano, M. S.; Blankschtein, D. *J. Am. Chem. Soc.* **2010**, *132*, 14638.
- (37) Margine, E. R.; Bocquet, M. L.; Blase, X. *Nano Lett.* **2008**, *8*, 3315.
- (38) Cognet, L.; Tsybolski, D. A.; Rocha, J. D. R.; Doyle, C. D.; Tour, J. M.; Weisman, R. B. *Science* **2007**, *316*, 1465.
- (39) Siitonen, A. J.; Tsybolski, D. A.; Bachilo, S. M.; Weisman, R. B. *Nano Lett.* **2010**, *10*, 1595.
- (40) Siitonen, A. J.; Tsybolski, D. A.; Bachilo, S. M.; Weisman, R. B. *J. Phys. Chem. Lett.* **2010**, *1*, 2189.
- (41) Englert, J. M.; Dotzer, C.; Yang, G. A.; Schmid, M.; Papp, C.; Gottfried, J. M.; Steinruck, H. P.; Spiecker, E.; Hauke, F.; Hirsch, A. *Nature Chem.* **2011**, *3*, 279.
- (42) Sharma, R.; Baik, J. H.; Perera, C. J.; Strano, M. S. *Nano Lett.* **2010**, *10*, 398.
- (43) Dreyer, D. R.; Park, S.; Bielawski, C. W.; Ruoff, R. S. *Chem. Soc. Rev.* **2010**, *39*, 228.
- (44) Shih, C.-J.; Lin, S.; Sharma, R.; Strano, M. S.; Blankschtein, D. *Langmuir* **2012**, *28*, 235.
- (45) Schneider, J.; Colombi Ciacchi, L. *J. Am. Chem. Soc.* **2012**, *134*, 2407.
- (46) Radadia, A. D.; Stavis, C. J.; Carr, R.; Zeng, H. J.; King, W. P.; Carlisle, J. A.; Aksimentiev, A.; Hamers, R. J.; Bashir, R. *Adv. Funct. Mater.* **2011**, *21*, 1040.
- (47) Liao, S.; Shnidman, Y.; Ulman, A. *J. Am. Chem. Soc.* **2000**, *122*, 3688.
- (48) Schneider, J.; Ciacchi, L. C. *J. Chem. Theory Comput.* **2010**, *7*, 473.
- (49) Steenackers, M.; Gigler, A. M.; Zhang, N.; Deubel, F.; Seifert, M.; Hess, L. H.; Lim, C. H. Y. X.; Loh, K. P.; Garrido, J. A.; Jordan, R.; Stutzmann, M.; Sharp, I. D. *J. Am. Chem. Soc.* **2011**, *133*, 10490.
- (50) Riccò, M.; Pontiroli, D.; Mazzani, M.; Choucair, M.; Stride, J. A.; Yazyev, O. V. *Nano Lett.* **2011**, *11*, 4919.
- (51) Lin, Y.-C.; Lu, C.-C.; Yeh, C.-H.; Jin, C.; Suenaga, K.; Chiu, P.-W. *Nano Lett.* **2011**, *12*, 414.
- (52) Karousis, N.; Tagmatarchis, N.; Tasis, D. *Chem. Rev.* **2010**, *110*, 5366.
- (53) Singh, P.; Campidelli, S.; Giordani, S.; Bonifazi, D.; Bianco, A.; Prato, M. *Chem. Soc. Rev.* **2009**, *38*, 2214.
- (54) Humphrey, W.; Dalke, A.; Schulten, K. *J. Mol. Graph. Model.* **1996**, *14*, 33.